

Control of a Rotating Variable-Length Tethered System

**Mischa Kim and Christopher D. Hall
Aerospace and Ocean Engineering
Virginia Polytechnic Institute and State University
Blacksburg, Virginia**

13th AAS/AIAA Space Flight Mechanics Meeting

Ponce, Puerto Rico

9-13 February 2003

AAS Publications Office, P.O. Box 28130, San Diego, CA 92198

CONTROL OF A ROTATING VARIABLE-LENGTH TETHERED SYSTEM

Mischa Kim* and Christopher D. Hall†

We develop and illustrate techniques to control the motion of a Tethered Satellite System (TSS) comprised of n point masses and interconnected arbitrarily by m idealized tethers. In particular, the control problem of a triangular and symmetrical TSS with $n = 3$ point masses and $m = 3$ tethers is discussed. The equations of motion are derived using Lagrange's equations. Several mission scenarios for a proposed NASA mission considering the operation of an infrared telescope are introduced and asymptotic tracking laws based on input-state feedback linearization are developed. Required thrust levels can be significantly decreased by using additional tether length control to keep the TSS in a state corresponding to an instantaneous relative equilibrium at any point in time during the mission.

INTRODUCTION

Over the past three decades, a variety of concepts have been proposed for space exploration using Tethered Satellite Systems (TSS). These include scientific experiments in the microgravity environment, upper atmospheric research, cargo transfer between orbiting bodies, generation of electricity, and deep space observation.¹⁻³ Numerous missions have already been launched to verify the tethered system concept for space application. Important milestones include retrieval of a tether in space (TSS-1, 1992), successful deployment of a 20 km tether in space (SEDS-1, 1993), closed-loop control of a tether deployment (SEDS-2, 1994), and operation of an electrodynamic tether used in both power and thrust mode (PMG, 1993).^{4,5} The idea of interconnecting spacecraft by means of lightweight deployable tethers has been proven to be particularly attractive also for space observations for various reasons. Variable-baseline interferometric observations can be achieved by a carefully controlled deployment/retrieval procedure of the tethers. In addition, the observational plane can be densely covered by spinning the tethered system. Lastly, the high levels of propellant consumption demanded by separated spacecraft in formation can be dramatically reduced by tension control of the interconnecting tethers.

The paper is organized as follows. To begin with, a brief description of the science mission which motivated this study is presented. In the following section some relevant papers and articles on the dynamics and control of TSS are presented. Subsequently, the system model is introduced and the motion equations are derived. Relative equilibria are identified and other possible mission scenarios are presented followed by a thorough discussion on control law development. Finally, the performance of the controllers are validated considering the different mission scenarios.

*Graduate Assistant, Department of Aerospace and Ocean Engineering, Virginia Polytechnic Institute and State University, Blacksburg, Virginia. mischa@vt.edu. Student Member AIAA, Student Member AAS.

†Associate Professor, Department of Aerospace and Ocean Engineering, Virginia Polytechnic Institute and State University, Blacksburg, Virginia. cdhall@vt.edu. Associate Fellow AIAA, Member AAS.

THE SPECS MISSION CONCEPT

NASA's future Earth and Space science missions involve formation flying of multiple coordinated spacecraft. Several space science missions include distributed instruments, large phased arrays of lightweight reflectors, and long variable baseline space interferometers. An array of collectors and combiner spacecraft will form variable-baseline space interferometers for a variety of science missions such as the *Submillimeter Probe of the Evolution of Cosmic Structure* (SPECS).⁶ This particular mission concept was initiated by a NASA science team and proposes a 1 km baseline submillimeter interferometer ($\lambda \approx 40 - 500 \mu m$). It comprises possibly as few as three 3 - 4 meter diameter mirrors and rotates about the primary optical axis collecting (3 - 0.25 eV) photons which are then preprocessed by a central beam collector. Since operating such systems in any kind of Earth orbit is not feasible due to extensive fuel consumption and unsatisfactory photon yield, the second Lagrangian point in the Sun-Earth system L_2 was chosen as the operational environment. The SPECS spacecraft formation is intended to be placed in a Halo orbit about this libration point.⁷

LITERATURE REVIEW

Researchers have studied the complex dynamics of TSS using a variety of models. From the initial studies, where tethers were modelled to be perfectly flexible and inextensible, attention was shifted towards more realistic models accounting for tether mass, elasticity, and flexibility.

Burov and Troger⁸ considered the problem of the motion of an orbital pendulum suspended on a massless inextensible tether. They investigated the existence of relative equilibria as well as sufficient conditions for their stability. Particular attention was paid to the study of coupling reactions, more precisely, the question of whether certain equilibria are not realizable because the tether does not support compression. Issues associated with the stability of such a simple TSS during station-keeping, deployment and retrieval were addressed by Liaw and Abed.⁹ They derived tension control laws to guarantee system stability during station keeping and hypothesized a constant angle control strategy for subsatellite deployment/retrieval. They proved that this control law results in stable deployment but unstable retrieval. Similar studies were performed by Akella,¹⁰ who investigated the dynamics and control problem for a single tether system using a system description based on Gates' NRL report.¹¹

Dignath and Schiehlen¹² presented a method of damping structural vibrations for a TSS modelled as a multibody system. They considered the tethered deorbit of a reentry capsule without an additional propulsion system. Active damping was provided by an actuator between a rigid body and the tether. The dynamics of a TSS using a discretized model of the tether was studied by de Matteis and de Socio.¹³ The characteristics of different spatial discretization procedures were compared to investigate the dynamics of the Space Pendulum and the Space String. They concluded that among the considered techniques the spectral collocation method provided excellent accuracy and sufficient convergence characteristics. The interesting concept of "offset" control was discussed in two articles by Pradhan et al.¹⁴ and Kalantzis et al.¹⁵ Offset control refers to the time-dependent variation of the tether attachment point at the platform. In the first article, this offset scheme was used for simultaneous control of platform and tether pitch motion. Also, the simultaneous regulation of the platform pitch and longitudinal tether vibrations was considered. Kalantzis et al. investigated the dynamics and control of a TSS with the spacecraft connected in series by flexible tethers. They developed two controllers for attitude and vibration control to deal with the complex motion excited from various maneuvers performed during the mission. A control algorithm based on feedback linearization was used for attitude control, whereas a linear quadratic Gaussian/loop-transfer recovery (LQG/LTR) strategy was chosen to actuate the offset point controller to address tether vibration control.

The dynamics and control problems associated with an Earth-orbiting, symmetrical, and triangular TSS were studied by DeCou.¹⁶ He derived a control strategy assuming the entire system to be rigid body in the presence of gravity gradient disturbances. The author showed that thrust and fuel levels are within state of the art for a 10 km baseline dumbbell-like interferometer operating in synchronous orbit. DeCou also introduced a method of damping tether vibrations using linear offset control. In another paper DeCou¹⁷ studied the static shape of such TSS assuming finite mass density of the tethers and under the influence of the centrifugal forces caused by the rotation of the system. Misra¹⁸ investigated equilibrium configurations and stability characteristics of a three-body TSS whose center of mass moves in a circular orbit around the Earth. For his analysis the tethers were assumed to have negligible mass and to be inextensible and rigid. In an earlier article, Misra et al.¹⁹ studied the attitude dynamics of a system modelled as an ideal double pendulum on a circular orbit. They considered constant as well as variable tether length dynamics simulations. For the constant length cases they studied equilibrium configurations and small motion around these configurations. Misra and Modi²⁰ investigated the dynamics of an ideal N -body TSS and developed linear control laws for in- and out-of-plane motions to control librational dynamics in the neighborhood of stable vertical equilibrium configuration in a circular orbit. The equations of motion of N -body TSS with flexible tethers using a continuum model were derived by Keshmiri and Misra²¹ for dynamics simulations. The motion equations were linearized for control and stability analysis purposes. Librational as well as longitudinal and transverse elastic frequencies of several multibody systems were obtained. Misra et al.²² considered the dynamics of a dumbbell TSS in the vicinity of the Earth-Moon Lagrangian points. Equilibrium configurations of the system near the libration points were determined and librational frequencies about the stable configurations were calculated. Also, an in-depth analysis of the coupled motion of the center of mass and the tether libration was carried out for the dynamics near the translunar Lagrangian point. The positional stability of the ideal dumbbell TSS located in the vicinity of a collinear Lagrangian point was analyzed by Farquhar.²³ The mass of the tethers was assumed to be negligible and also the tension in the tethers was assumed to always be present. He showed that stability can be achieved using a linear control law for the tether length.

Extensive research addressed basic TSS dynamics and control problems, whereas little attention has been paid so far to the controlled motion of a complex TSS in orbits around the second Lagrangian point in the Sun-Earth system. This paper is a first step to gather a thorough understanding of the dynamics of such systems for future deep-space exploration. In the following section the system model is introduced for a TSS comprised of n point masses and m tethers.

SYSTEM MODEL AND EQUATIONS OF MOTION

In this section equations of motions (EOM) of the system are formulated using Gates' system description.¹¹ The mechanical system considered is shown in Figure 1. It is comprised of a system of n point masses interconnected arbitrarily by m idealized tethers. The tethers are assumed to be massless and extensible capable of exerting force only along the straight-line connecting the respective masses. Also, the tethers do not support compression or any components of shear forces or bending moments and are therefore assumed to be perfectly flexible. The constitutive character for the tethers is taken as visco-elastic, allowing intrinsic energy dissipation. Since the system is ultimately being operated at the second Lagrangian point L_2 in the Sun-Earth system, gravitational and other environmental forces are assumed to be negligible.

The EOM are derived using Lagrange's equations defined in a "prescribed motion" reference frame \mathcal{F}_P rather than in an inertial reference frame \mathcal{F}_I . Cylindrical coordinates relative to \mathcal{F}_P are chosen to describe the position of the point masses. As illustrated in Figure 1, r_i , θ_i , and z_i are the radial distance in the $e_x e_y$ plane, the angle between the e_x -axis and the projection of the

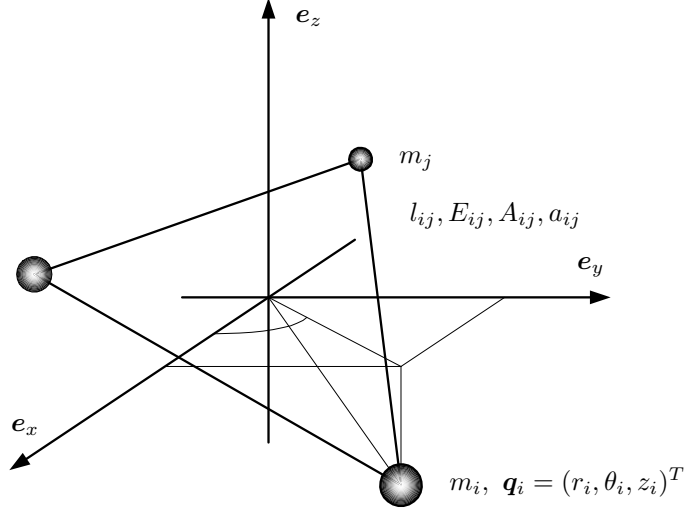


Figure 1: System model in cylindrical coordinates.

position vector \mathbf{q}_i onto the $e_x e_y$ plane, and the axial distance in e_z direction of the point mass m_i , respectively. The formulation is generalized by the addition of rheonomic constraints to allow for specification of any or all of the degrees of freedom. The motion equations for the controlled system are

$$\mathbf{M}_i \ddot{\mathbf{q}}_i = \mathbf{Q}_i^{(e)} + \mathbf{N}_i + \mathbf{S}_i + \mathbf{U}_i, \quad i = 1, 2, \dots, n \quad (1)$$

where

$$\mathbf{M}_i = m_i \begin{bmatrix} 1 & 0 & 0 \\ 0 & r_i^2 & 0 \\ 0 & 0 & 1 \end{bmatrix}, \quad \mathbf{q}_i = \begin{pmatrix} r_i \\ \theta_i \\ z_i \end{pmatrix}, \quad \mathbf{Q}_i^{(e)} = \begin{pmatrix} F_{ri} \\ r_i F_{ti} \\ F_{zi} \end{pmatrix}, \quad \mathbf{S}_i = \mathbf{Q}_i^{(i)} \quad (2)$$

In equations (1) \mathbf{M}_i , \mathbf{q}_i , $\mathbf{Q}_i^{(e)}$, \mathbf{N}_i , \mathbf{S}_i , and \mathbf{U}_i are the mass matrix, the vector of generalized coordinates, and the vectors of external, coupling, spring (or internal), and control forces for the i th point mass, respectively. For later analysis it is pointed out that the spring forces in equations (1) are obtained assuming a Kelvin–Voigt constitutive law; that is, the tensile stress, τ_{ij} , and the longitudinal strain, ϵ_{ij} , are related by

$$\tau_{ij} = E_{ij}(\epsilon_{ij} + a_{ij}\dot{\epsilon}_{ij}) \quad i, j = 1, 2, \dots, n \text{ and } i \neq j \quad (3)$$

where E_{ij} is the effective Young's modulus and a_{ij} is a constant dissipation parameter for the tether connecting point masses m_i and m_j . The longitudinal strain in the tether is defined as

$$\epsilon_{ij} = \frac{l_{ij} - d_{ij}}{d_{ij}} \quad (4)$$

where l_{ij} and d_{ij} are the actual and the unstrained tether length, respectively. Hence, if A_{ij} is the effective cross sectional area of the tether then the tension is given by

$$f_{ij} = \begin{cases} A_{ij}\tau_{ij} & \text{if } \epsilon_{ij} \geq 0 \text{ and } \tau_{ij} \geq 0 \\ 0 & \text{otherwise} \end{cases} \quad (5)$$

which introduces discontinuities since the tethers do not support compression. Defining the vector of generalized coordinate vectors for the system as

$$\mathbf{q} = (\mathbf{q}_1^T, \mathbf{q}_2^T, \dots, \mathbf{q}_{n-1}^T, \mathbf{q}_n^T)^T \quad (6)$$

equations (1) can be combined to yield

$$\mathbf{M}\ddot{\mathbf{q}} = \mathbf{Q}^{(e)} + \mathbf{N} + \mathbf{S} + \mathbf{U} \quad (7)$$

where

$$\mathbf{M} = \begin{bmatrix} \mathbf{M}_1 & \mathbf{0}_3 & \dots & \mathbf{0}_3 \\ \mathbf{0}_3 & \mathbf{M}_2 & \dots & \mathbf{0}_3 \\ \vdots & \vdots & \ddots & \vdots \\ \mathbf{0}_3 & \mathbf{0}_3 & \dots & \mathbf{M}_n \end{bmatrix}, \mathbf{Q}^{(e)} = \begin{pmatrix} \mathbf{Q}_1^{(e)} \\ \mathbf{Q}_2^{(e)} \\ \vdots \\ \mathbf{Q}_n^{(e)} \end{pmatrix}, \mathbf{N} = \begin{pmatrix} \mathbf{N}_1 \\ \mathbf{N}_2 \\ \vdots \\ \mathbf{N}_n \end{pmatrix}, \mathbf{S} = \begin{pmatrix} \mathbf{S}_1 \\ \mathbf{S}_2 \\ \vdots \\ \mathbf{S}_n \end{pmatrix}, \mathbf{U} = \begin{pmatrix} \mathbf{U}_1 \\ \mathbf{U}_2 \\ \vdots \\ \mathbf{U}_n \end{pmatrix} \quad (8)$$

where $\mathbf{0}_3$ is the 3×3 null matrix. Notice that equations (7) are readily integrated after being transformed to a set of $2 \times 3n$ first order ODEs; that is, defining $\mathbf{x} = x_i = (\mathbf{q}, \dot{\mathbf{q}})^T$ equations (7) can be written in compact form as

$$\dot{\mathbf{x}} = \mathbf{f}(\mathbf{x}), \quad \text{where} \quad \mathbf{f}(\mathbf{x}) = \begin{pmatrix} \dot{\mathbf{q}} \\ \mathbf{M}^{-1}(\mathbf{Q}^{(e)} + \mathbf{N} + \mathbf{S} + \mathbf{U}) \end{pmatrix} \quad (9)$$

For the subsequent analysis a TSS comprised of $n = 3$ point masses and $m = 3$ tethers is considered.

RELATIVE EQUILIBRIA

Reviewing Gates' system description we note that the spring forces appearing in equations (1) can be written as

$$\mathbf{S}_i = \sum_{\substack{j=1 \\ j \neq i}}^{n=3} \frac{f_{ij}}{l_{ij}} \begin{pmatrix} \sigma_{ij} \\ \tau_{ij} \\ \zeta_{ij} \end{pmatrix} \quad (10)$$

where we have introduced the quantities

$$\begin{aligned} \sigma_{ij} &= r_j \cos(\theta_j - \theta_i) - r_i \\ \tau_{ij} &= r_i r_j \sin(\theta_j - \theta_i) \\ \zeta_{ij} &= z_j - z_i \end{aligned} \quad (11)$$

Additionally, in the rotating reference frame $\mathcal{F}_{\mathcal{P}}$ the relative equilibrium motion satisfies

$$\dot{\mathbf{x}}_{\mathcal{P}}^e = \mathbf{f}_{\mathcal{P}}(\mathbf{x}_{\mathcal{P}}^e) = \mathbf{0} \quad (12)$$

where the superscript denotes the relative equilibrium state. Assuming a perfectly symmetrical ($n = 3, m = 3$) TSS it is sufficient to analyze either of the subsystems described by equations (1). Temporarily dropping the point mass subscript notation and noting that $|\theta_j - \theta_i| = 2\pi/3$ we find three conditions for each of the three point masses of the form

$$r^e = \text{const.} \quad (13)$$

$$\dot{\theta}^e(r^e) = \sqrt{\frac{\sqrt{3}EA(\sqrt{3}r^e - d)}{mr^e d}}, \quad (\text{note: } l^e = \sqrt{3}r^e) \quad (14)$$

$$z^e = \text{const.} \quad (15)$$

Therefore, the relative equilibrium angular velocity for the TSS is

$$\dot{\theta}^e(l^e) = \sqrt{\frac{3EA(l^e - d)}{ml^e d}} \quad (16)$$

which shows that the rotating TSS has to be under tension ($l^e > d$).

MISSION SCENARIOS FOR SPECS

This section discusses different mission scenarios to validate the control law developed in the following section. The first scenario deals with the control of the TSS to a specific relative equilibrium. Mission scenarios 2 and 3 describe trajectory designs which are relevant for the SPECS mission. To decrease overall thrust levels, refinements to the control laws are introduced which include additional tether length control.

Mission scenario 1: Stabilization of a relative equilibrium motion

The first mission scenario considers the stabilization of a particular relative equilibrium motion of the TSS. This case is of importance for those phases during the sequence of observations when the satellite formation needs to be reoriented to point at specific targets of interest. Using equations (13)–(15) the desired trajectories $\mathbf{y}_{i,d}$ for the point masses m_i are

$$\mathbf{y}_{i,d} = (r_{i,d}, \theta_{i,d}, z_{i,d})^T = \left(r^e, t\dot{\theta}^e + (i-1)\theta_{\Delta}, z^e \right)^T \quad i = 1, 2, 3 \quad (17)$$

where $\theta_{\Delta} = 2\pi/3$ and with appropriately chosen initial conditions.

Mission scenario 2: Simple tether deployment/retrieval mission

The above mission scenario can be extended to include a tether deployment/retrieval procedure which allows the system to (partially or fully) cover the observational plane. Figure 2 shows the time history of the desired trajectory and the trace of one of the point masses for the proposed mission. Note that the angular velocity of the system is chosen to be constant during the entire mission. Also, the time rate of change of the radial distance of the point masses is assumed to be constant during tether deployment/retrieval. Obviously, depending on the ratio (radial deployment/retrieval rate):(system angular velocity) partial or full coverage of the observational plane is obtained for a given mirror diameter.

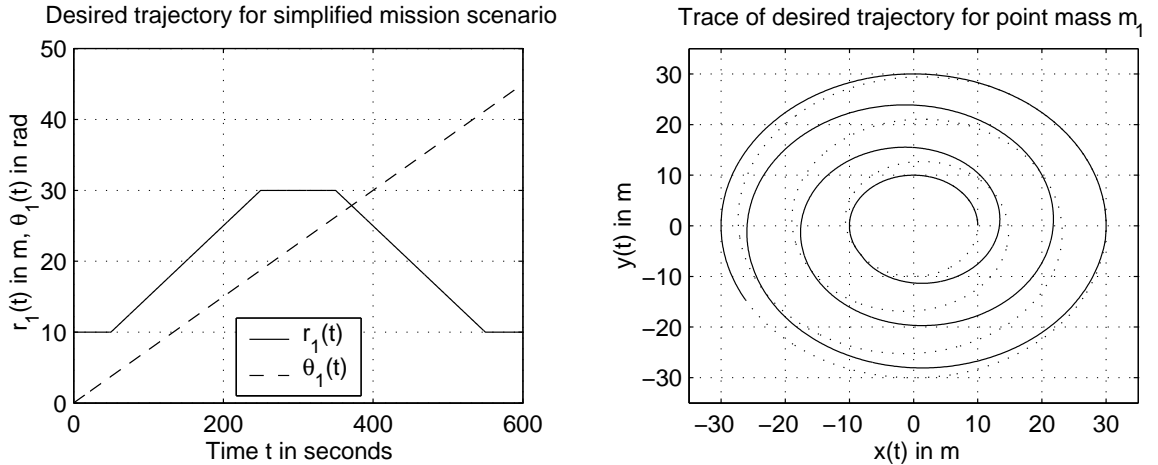


Figure 2: Desired trajectory of point mass m_1 for simplified mission scenario. Similar plots are obtained for m_2 and m_3 due to system symmetry. The system angular velocity as well as the deployment/retrieval rate are assumed to be constant.

It is important to note at this point, that for the mission scenario described different prescribed tether length control laws can be formulated. To study the improvement on thrust savings two

particular tether length control laws are chosen for comparison. The first control law assumes a simple linear relationship between the radial distance of the point masses and the tether length whereas the second control law prescribes a tether length history such as to keep the TSS in a relative equilibrium at any point in time during the mission.

Mission scenario 3: SPECS relevant mission scenario

Further refinements to possible mission trajectories can be made by requiring the mirrors to cover the observational plane using a more efficient pattern like an Archimedes spiral, which is described in polar coordinates by $r = a\theta$, where a is an arbitrary constant. For this particular mission scenario an additional scientifically motivated constraint is formulated to define a specific trajectory unambiguously. In particular, we require that the instantaneous tangential velocity of each of the three point masses never exceeds a maximal value v_{max} . Figure 3 shows an example of such a mission trajectory. Temporarily dropping the subscript notation due to system symmetry the three positional constraints for the TSS are

$$dr = \frac{3D}{2\pi}d\theta, \quad r\dot{\theta} = v_{max}, \quad \text{and} \quad z = \text{const.} \quad (18)$$

where D is the mirror diameter. These constraints can be combined to yield

$$r\dot{r} = \frac{1}{2} \frac{d}{dt} (r^2) = \frac{3Dv_{max}}{2\pi} =: \alpha = \text{const.} \quad (19)$$

Therefore, the radial function has to be of the form $r = c_1\sqrt{t + c_2}$. Substituting this ansatz function into equations (18) and (19) eventually results in

$$\begin{aligned} r_d &= \sqrt{r_{0+}^2 + 2\alpha t} \\ \theta_d &= \theta_{0+} - \frac{v_{max}}{\alpha} \left(r_{0+} - \sqrt{r_{0+}^2 + 2\alpha t} \right) \\ z_d &= z_{0+} \end{aligned} \quad (20)$$

where r_{0+} , θ_{0+} and z_{0+} are the initial conditions for deployment. Equations (20) describe the time history of each of the point masses during tether deployment. A similar analysis for the retrieval procedure eventually yields for the desired deployment/retrieval trajectories

$$\begin{aligned} r_{i,d} &= \sqrt{r_{0\pm}^2 \pm 2\alpha t} \\ \theta_{i,d} &= \theta_{0\pm} + (i-1)\theta_{\Delta} - \frac{v_{max}}{\alpha} \left(\pm r_{0\pm} \mp \sqrt{r_{0\pm}^2 \pm 2\alpha t} \right), \quad i = 1, 2, 3 \\ z_{i,d} &= z_{0\pm} \end{aligned} \quad (21)$$

In equations (21) the upper signs hold for tether deployment, the lower signs hold for tether retrieval phases. Initial conditions for both procedures are denoted by $\mathbf{q}_{0\pm} = (r_{0\pm}, \theta_{0\pm}, z_{0\pm})^T$, where the plus/minus sign indicates tether deployment/retrieval.

Improvements to the SPECS trajectory: Introduction of smoothing functions

Discontinuities in the functions describing the desired trajectory result in undesirable discontinuities in requested controls. One way to deal with this issue is to introduce smoothing functions into the desired trajectory during critical periods of time. For the SPECS trajectory developed in the

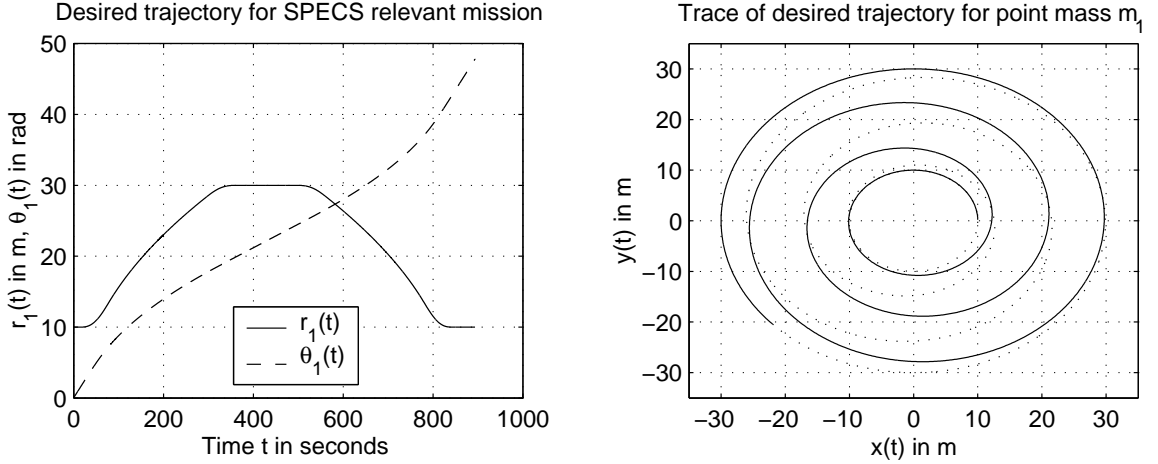


Figure 3: Desired trajectory for a SPECS relevant mission scenario. Similar plots are obtained for m_2 and m_3 due to system symmetry. Full coverage of the observational plane is guaranteed for a given mirror diameter and for a chosen constant tangential velocity of the point masses.

previous section this matter is complicated by the fact that the radial and the angular component of the trajectory are not independent of each other ($r\dot{\theta} = v_{max}$). Integrating an ansatz function of the form

$$\ddot{\theta}_{i,d} = C_1 (t - t_s^i)^3 + C_2 (t - t_s^i)^2 + C_3 (t - t_s^i), \quad i = 1, 2, 3 \quad (22)$$

yields algebraic expression for $\ddot{\theta}_{i,d}$ and $\dot{\theta}_{i,d}$. In equations (22) t_s^i denotes the starting time of the smoothing process. Constants C_i are derived formulating appropriate boundary transition conditions at the endpoints of the smoothing interval at $t = t_s^i$ and $t = t_s^f$. For example, for the initial segment of the SPECS trajectory where the system changes from a steady-spin motion into the tether deployment phase (Figure 4) these conditions yield

$$\begin{aligned} \text{at } t = t_s^i : \quad & \dot{\theta}_{i,d} = \frac{v_{max}}{r_{0+}}, \quad \ddot{\theta}_{i,d} = 0, \quad \dddot{\theta}_{i,d} = 0, \\ \text{at } t = t_s^f : \quad & \dot{\theta}_{i,d} = \frac{v_{max}}{r_\star}, \quad \ddot{\theta}_{i,d} = \frac{-\alpha v_{max}}{r_\star^3}, \quad \dddot{\theta}_{i,d} = \frac{3\alpha^2 v_{max}}{r_\star^5}, \quad \text{where } r_\star = \sqrt{r_{0+}^2 + 2\alpha(t_s^f - t^\star)} \end{aligned}$$

and where t^\star denotes the starting time of the tether deployment phase for the non-smooth SPECS trajectory (Figure 4). Coefficients C_1 through C_3 are uniquely determined by the three conditions at time $t = t_s^f$. Note that the latter two conditions at $t = t_s^f$ are trivially satisfied whereas the first condition fixes an additional integration constant C_4 which appears in the analytic expression for $\dot{\theta}_{i,d}$. Considering constraint $r\dot{\theta} = v_{max}$ yields functions $r_{i,d}$, $\dot{r}_{i,d}$ and $\ddot{r}_{i,d}$. Note that the special choice of $\ddot{\theta}_{i,d}$ guarantees that a) $\ddot{r}_{i,d} = \ddot{r}_{i,d}(\dot{\theta}_{i,d}, \ddot{\theta}_{i,d}, \dddot{\theta}_{i,d})$ are continuous and therefore $\dot{r}_{i,d}$, $r_{i,d}$ are smooth and b) $\dot{\theta}_{i,d} \neq 0$ and therefore $r_{i,d}$ bounded for $t \in [t_s^i, t_s^f]$. Figures 4(a,b) show that equations (22) have either two or one zeros in the interval $t \in (t_s^i, t_s^f)$ when used as proper smoothing functions (dashed lines) for the SPECS trajectory (solid lines). Figure 4(c) shows the impossible case where $\ddot{\theta}_{i,d} \neq 0$ for $t \in (t_s^i, t_s^f)$.

In the next section the tools necessary to develop a nonlinear feedback controller based on input-state feedback linearization are introduced. In particular, a regulator and an asymptotic tracking law are derived for the general TSS consisting of n point masses interconnected by m tethers.

CONTROL LAW DEVELOPMENT

When the requirements on the system performance are mild and the system operates in a small

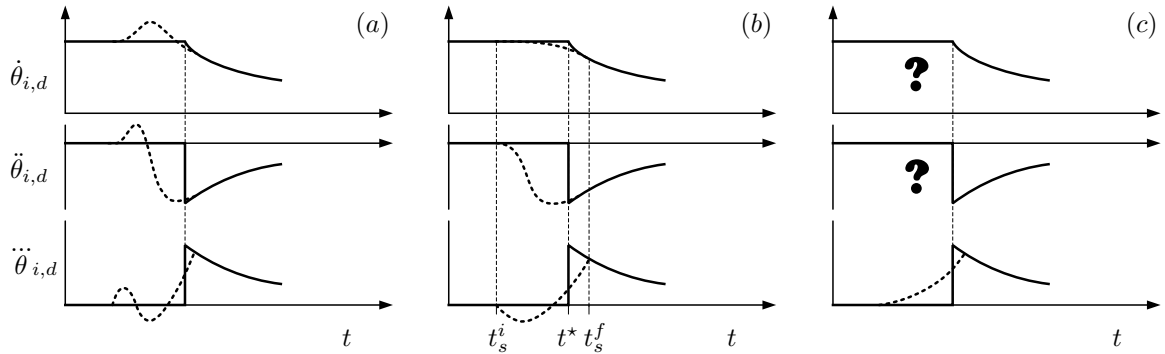


Figure 4: Time derivatives of $\theta_{i,d}$ for initial segment of the non-smooth SPECS trajectory (solid lines). Dashed lines denote smoothing functions for the case when equations (22) have two (a), one (b) or no zeros (c) in the time interval $t \in (t_s^i, t_s^f)$. Case (c) is not possible.

dynamic regime linear controllers are often acceptable. However, in many systems the nonlinearities are so dominant that these controllers can hardly meet requirements on system performance. In these cases development of control approaches that incorporate the nonlinear dynamics into the design process becomes necessary.^{24–27} One such approach is feedback linearization.²⁸ Unlike the Jacobian linearization approach, which ignores all higher-order terms of the system, this technique utilizes the feedback and a coordinates transformation to render the given system one with linear input–output dynamics. Then linear control techniques can be further applied to address design issues.

In the following sections a regulator and an asymptotic tracker control law based on input–state feedback linearization are developed. For this analysis the positions of the point masses m_i are chosen as outputs; that is, $\mathbf{y}_i \equiv \mathbf{q}_i = (r_i, \theta_i, z_i)^T$, $i = 1, 2, 3$. Also, due to the particular choice of control inputs in equations (1) it is straightforward to show that the system is completely controllable.

Regulator design using input–state feedback linearization

Recall that the investigated system is a so-called *square* system (number of inputs equals the number of outputs) of the form

$$\begin{aligned} \dot{\mathbf{x}} &= \mathbf{f}(\mathbf{x}) + \mathbf{G}(\mathbf{x})\mathbf{u} \\ \mathbf{y} &= \mathbf{h}(\mathbf{x}) \end{aligned} \quad (23)$$

where $\mathbf{x} \in \mathbb{R}^N$, $\mathbf{u} = (\mathbf{u}_1^T, \dots, \mathbf{u}_p^T)^T \in \mathbb{R}^P$, $\mathbf{y} = (\mathbf{y}_1^T, \dots, \mathbf{y}_p^T)^T \in \mathbb{R}^P$, and \mathbf{f} and \mathbf{g}_j are assumed to be smooth vector fields and h_i to be smooth functions in some domain D_0 . Note that for the TSS, $N = 2 \times 3n = 18$ and $P = 3n = 9$.

Similar to the case of single–input single–output (SISO) systems the input–state linearization problem for the multi–input multi–output (MIMO) system can be tackled by successively differentiating the output vector. To describe the procedure it is convenient to extend the notion of relative degree to the MIMO case.

Definition The system (23) is said to have *vector relative degree* $\gamma_1, \gamma_2, \dots, \gamma_p$ at $\mathbf{x}_0 \in D_0$ if

$$\mathcal{L}_{\mathbf{g}_j} \mathcal{L}_f^k h_i(\mathbf{x}) \equiv 0, \quad 0 \leq k \leq \gamma_i - 2 \quad (24)$$

for $i, j = 1, 2, \dots, P$ for all \mathbf{x} in a neighborhood of \mathbf{x}_0 and the matrix

$$\mathbf{A}(\mathbf{x}) := \begin{bmatrix} \mathcal{L}_{g_1} \mathcal{L}_f^{\gamma_1-1} h_1 & \dots & \mathcal{L}_{g_P} \mathcal{L}_f^{\gamma_1-1} h_1 \\ \vdots & \ddots & \vdots \\ \mathcal{L}_{g_1} \mathcal{L}_f^{\gamma_P-1} h_P & \dots & \mathcal{L}_{g_P} \mathcal{L}_f^{\gamma_P-1} h_P \end{bmatrix} \quad (25)$$

is nonsingular at \mathbf{x}_0 and where $\mathcal{L}_\phi^k \chi_i(\mathbf{x})$ is the k th Lie derivative of a function χ_i with respect to a vector field ϕ .²⁵

Note that similar to the case of SISO systems, if a MIMO system of the form (23) has a well defined vector relative degree and furthermore is such that $\gamma_1 + \gamma_2 + \dots + \gamma_P = N$ then the system is input–state linearizable. This linearization is realized by first choosing a new set of coordinates $\psi_{i+Pj_k} = \mathbf{T}x_{i+Pj_k} \equiv \mathcal{L}_f^{j_k} h_i(\mathbf{x})$, $j_k = 0, \dots, \gamma_k - 1$, $k = 1, \dots, P$ with a jacobian matrix which is nonsingular at \mathbf{x}_0 and therefore qualifies as a local coordinates transformation in a neighborhood of \mathbf{x}_0 . Then the feedback control law has the form $\mathbf{u}(\boldsymbol{\psi}) = \mathbf{A}(\boldsymbol{\psi})^{-1}(-\mathbf{b}(\boldsymbol{\psi}) + \mathbf{v}(\boldsymbol{\psi}))$ where

$$\mathbf{A}(\boldsymbol{\psi}) = a_{ij}(\boldsymbol{\psi}) = \mathcal{L}_{g_j} \mathcal{L}_f^{\gamma_i-1} h_i \circ \mathbf{T}^{-1} \boldsymbol{\psi} \quad \text{and} \quad \mathbf{b}(\boldsymbol{\psi}) = b_i(\boldsymbol{\psi}) = \mathcal{L}_f^{\gamma_i} h_i \circ \mathbf{T}^{-1} \boldsymbol{\psi} \quad (26)$$

Recall that with $\mathbf{x}_i = (r_i, \theta_i, z_i, \dot{r}_i, \dot{\theta}_i, \dot{z}_i)^T = (\mathbf{q}_i, \dot{\mathbf{q}}_i)^T$ and due to the symmetry of the system the equations of motions of the TSS can be analyzed as three subsystems each of which describes the dynamics of one of the point masses. The controlled motion equations are

$$\dot{\mathbf{x}}_i = \left(\mathbf{M}_i^{-1} \left(\mathbf{Q}_i^{(e)} + \mathbf{N}_i + \mathbf{S}_i + \mathbf{U}_i \right) \right), \quad i = 1, 2, 3 \quad (27)$$

where \mathbf{U}_i , $i = 1, 2, 3$ are the control inputs. Note that due to the particular choice of inputs and outputs the system is already in normal form. Therefore, the coordinates transformation $\psi_{i+Pj_k} = \mathbf{T}x_{i+Pj_k} \equiv \mathcal{L}_f^{j_k} h_i(\mathbf{x})$, $j_k = 0, \dots, \gamma_k - 1$ is simply the unit transformation $\boldsymbol{\psi} = \mathbf{x}$. As can be easily checked, each of the subsystems decouples into three subsystems each of relative degree $\gamma'_i = 2$, $i = 1, 2, 3$. Therefore, the complete system (27) is input–state linearizable. Hence, the equations of motion in the new coordinates can be written in compact form as

$$\dot{\boldsymbol{\psi}} = \mathbf{b}(\boldsymbol{\psi}) + \mathbf{A}(\boldsymbol{\psi})\mathbf{u}(\boldsymbol{\psi}) \quad (28)$$

With the particular simple coordinates transformation it then follows from the normal form equations that the feedback control laws given by

$$\mathbf{u}(\boldsymbol{\psi}) = \mathbf{A}(\boldsymbol{\psi})^{-1}(-\mathbf{b}(\boldsymbol{\psi}) + \mathbf{v}(\boldsymbol{\psi})) \equiv \mathbf{A}(\mathbf{x})^{-1}(-\mathbf{b}(\mathbf{x}) + \mathbf{v}(\mathbf{x})) = \mathbf{u}(\mathbf{x}) \quad (29)$$

yield a linear system of equations, with \mathbf{v} chosen to place the poles of the resulting input–output dynamics.

It is crucial to note that the conditions stated in the definition above are not necessarily strictly fulfilled at all times during a mission due to the discontinuities in the tethers. However, even though these critical phases during tether deployment/retrieval are likely to occur in a real observation they are by all means rare events and are therefore assumed to be negligible for the present analysis. Also, a more complex coupled control law for the point masses and the tether tension/length should be capable of keeping the system under tension during an entire mission. This issue will be addressed by the authors at a later point in time.

Asymptotic tracking

Due to the special structure of the feedback linearized system as discussed in the previous section – the inputs directly govern the motion of the outputs – the design of the controller for an *asymptotic*

tracking problem is straightforward. That is, given a dynamic system described by equations (23) and a desired trajectory \mathbf{y}_d , find a control law for the input \mathbf{u} such that, starting from any initial state in a domain D_0 , the tracking error vector $\mathbf{e} = \mathbf{y} - \mathbf{y}_d$ goes to zero, while the state remains bounded. Obviously, asymptotic stability of the error vectors is guaranteed by requiring

$$e_i^{(\rho)} + a_{i,\rho-1}e_i^{(\rho-1)} + \dots + a_{i,1}e_i^{(1)} + a_{i,0}e_i = 0 \quad i = 1, 2, \dots, P \quad (30)$$

where $e_i^{(\rho)}$ denotes the ρ th-order derivative of the i th component of the error vector with $\omega_i^{(\rho)} = v_i$ and where the $a_{i,j}$ ($i = 1, 2, \dots, P$, $j = 0, 1, \dots, \rho - 1$) are chosen such that the polynomials

$$p_i(\lambda) = \lambda^\rho + a_{i,\rho-1}\lambda^{\rho-1} + \dots + a_{i,1}\lambda + a_{i,0} \quad i = 1, 2, \dots, P \quad (31)$$

have all their roots strictly in the left-half plane. Similarly, equations (30) in transformed coordinates are satisfied if and only if

$$\left(v_i - \omega_{d,i}^{(\rho)}\right) + \alpha_{i,\rho-1}\varepsilon_i^{(\rho-1)} + \dots + \alpha_{i,1}\varepsilon_i^{(1)} + \alpha_{i,0}\varepsilon_i = 0 \quad i = 1, 2, \dots, P \quad (32)$$

where ε , ω , and $\alpha_{i,j}$ are the tracking error vector, the output vector, and the control parameters in transformed coordinates, respectively, with $\varepsilon^{(\rho)} = \omega^{(\rho)} - \omega_d^{(\rho)} = \mathbf{v} - \omega_d^{(\rho)}$. Solving for v_i gives the desired control law

$$v_i = \omega_{d,i}^{(\rho)} - \left\{ \alpha_{i,\rho-1}\varepsilon_i^{(\rho-1)} + \dots + \alpha_{i,1}\varepsilon_i^{(1)} + \alpha_{i,0}\varepsilon_i \right\}^\ddagger \quad i = 1, 2, \dots, P \quad (34)$$

As mentioned previously, one of the mission scenarios considered in this paper requires the system to follow the motion of a specific relative equilibrium. For this case, the desired trajectories $\omega_{i,d} \equiv \mathbf{y}_{i,d}$ can be written as

$$\omega_{i,d} = (r_{i,d}, \theta_{i,d}, z_{i,d})^T = (r^e, t\dot{\theta}^e + (i-1)\theta_\Delta, z^e)^T \quad i = 1, 2, 3 \quad (35)$$

and the control laws (34) are easily obtained.

Gain selection for the linear controller

In this section we present a way to choose controller parameters for the linear controller derived in the previous section. Equations (30) show that the particular choice of linear feedback terms decouples the individual coordinate directions and a set of structurally similar equations are obtained. It is therefore sufficient to analyze only one of these equations. Temporarily dropping the subscript notation and noting that only time derivatives up to an order of $\rho = 2$ are involved the linear system can be written as

$$\ddot{e} + a\dot{e} + be = 0 \quad (36)$$

A powerful tool for linear control system design is the root-locus method to obtain the system root locations relative to a single parameter. One way to identify this particular parameter in a second order system represented by equation (36) is to rewrite its characteristic polynomial as

$$s^2 + as + b = s^2 + a(s + b/a) = 0 \quad \text{or} \quad s^2 + K(s + c) = 0 \quad \text{with } K = a, \text{ and } c = b/a \quad (37)$$

[†]Note, that the *stabilization problem* can be viewed as a special case of the asymptotic tracking problem when the reference input is $\omega_d = \mathbf{0}$. In this case the control law (34) becomes

$$v_i = - \left\{ \alpha_{i,\rho-1}\omega_i^{(\rho-1)} + \dots + \alpha_{i,1}\omega_i^{(1)} + \alpha_{i,0}\omega_i \right\} \quad i = 1, 2, \dots, P. \quad (33)$$

For $a > 0$ and $b > 0$ the roots of this characteristic equation are all strictly in the left-half plane and the system is asymptotically stable. Figure 5(a) shows the corresponding root-locus plot. The roots of the characteristic equation are

$$s_{1,2} = \frac{-a \pm \sqrt{a^2 - 4b}}{2} \quad (38)$$

Aiming for a critically damped system we note that the roots and the parameter K for this case are

$$s_{1,2}^c = -\frac{a}{2} = -2c, \quad K^c = 4c \quad (39)$$

In Figure 5(a) this point is found at the intersection of the circle with the real axis in the left-half plane. Note that the size of the circle depends on the ratio $c = b/a$ whereas the exact location of the roots are a function of a only once c is fixed. It is therefore reasonable to choose $K (= a)$ as the representative parameter since the size of the circle can be chosen as a function of system performance criteria such as time-domain specifications for a step response (Figures 5(b,c)). For second order systems a standard routine to describe the transient response to a step function is to specify parameters such as rise time t_r , settling time t_s and overshoot M_p . These parameters are then translated into corresponding parameters in the s -plane using²⁹

$$\omega_n \approx \frac{1.8}{t_r}, \quad \sigma \approx \frac{4.6}{t_s}, \quad \varphi = \sin^{-1} \zeta, \quad \text{where } \zeta = \sqrt{\frac{\alpha}{1 + \alpha}}, \quad \text{and } \alpha = \left(\frac{\ln M_p}{\pi}\right)^2 \quad (40)$$

Replacing the first three (approximately) equal-signs in equations (40) by greater-than-signs restricts the region of possible root locations in the s -plane as shown in Figure 5(b). Since we are aiming for a critically damped system it is preferable to choose c (and therefore K or a) as small as possible to minimize the control input (thrust) without violating the performance constraints (Figure 5(c)).

In the following section candidates for relevant mission scenario are presented and the performance of the controllers discussed.

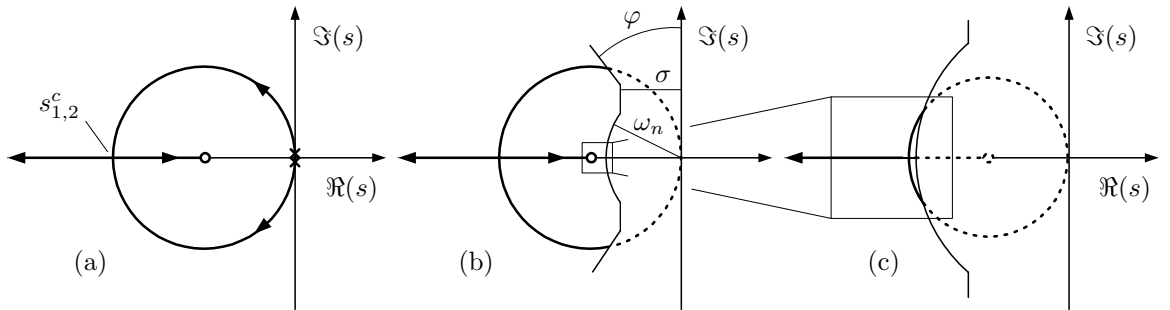


Figure 5: Linear controller gain selection. Root-locus plot for a second order system with a characteristic polynomial of the form $s^2 + as + b = 0$, $a > 0$, $b > 0$ (a). Imposing transient requirements on the system restricts the region of possible root locations in the s -plane (b) which in turn can be used to select control parameters (c).

EXAMPLES

We developed and implemented a generic simulation code in C++ to validate the performance of the control laws presented in the previous sections. In particular, the mission scenarios described earlier were used to define desired trajectories. System and simulation parameters are listed in Table 1.

The integration step size was chosen based on a comparison of total thrust levels obtained during similar simulation runs and was found to yield results with satisfying accuracy. Control parameters were chosen such as to yield satisfactory transient behavior for the choice of system and simulation parameters. For the perturbed initial conditions response simulation the perturbation vectors were generated randomly with an upper bound of $\delta x \leq 10^{-3}$ for each element of the vectors. Finally, the initial and final radial distance of the point masses for mission scenarios 2 and 3 were chosen to be $R_0 = r_{0+} = 10$ m and $R_f = r_{0-} = 30$ m.

Table 1: System and simulation parameters.

Point masses m_i in kg	50.0	Integration time step dt in s	0.02
Mirror diameters D_i in m	3.0	IC disturbances $\delta x_{i,j}$ in $[\delta x_{i,j}]$	$\leq 10^{-3} \times \mathbf{1}_9$
Young's moduli E_{ij} in N/mm ²	10,000	Rise time (step response) t_r in s	2.0
Tether cross sections A_{ij} in mm ²	0.79	Settling time (step response) t_s in s	5.0
Damping parameters a_{ij} in s	0.0	Overshoot (step response) M_p in %	0.0
Initial radial distance R_0 in m	10.0	Control parameters $\alpha_{i,1}$ ($= a$) in $[\alpha_{i,1}]$	2.0
Final radial distance R_f in m	30.0	Control parameters $\alpha_{i,0}$ ($= b$) in $[\alpha_{i,0}]$	1.0

Figures 6–9 show simulation results for the various mission scenarios. The initial conditions perturbation response is illustrated in Figure 6. The randomly disturbed TSS approaches the relative equilibrium motion with a steady state radial distance of the point masses of $r^e = 10$ m within a period of about 5.0 s. During this process the thrust requirements in the radial direction are significantly lower than they are in the azimuthal direction which is in part due to the effect of the tethers.

The results for mission scenario 2 are illustrated in Figure 7. The tether length control law is a simple linear and constant relationship between the radial distance of the point masses and the unstrained tether lengths. As a result, during deployment/retrieval of the tethers the overall tether tension decreases/increases relatively which in turn requires increasing/decreasing thrust levels. The mission duration is approximately 900 s, the position errors for this particular setup are all in the centimeter range. Required controls in the r and θ directions range up to 15 N and 20 N, respectively. This particular case also shows that the choice of the constant relating the unstrained tether length to the actual particle-to-particle distance is suboptimal. The direction of the radial control component remains negative during the mission, and the system steadily diverges from a possible state of a relative equilibrium during deployment.

Since such a simple mission trajectory does not guarantee time efficient and complete coverage of the observational plane we introduced the more natural Archimedes spiral pattern as the desired trajectory in a previous section. Figure 8 shows simulation results for mission scenario 3 using the simple linear tether length control law. Similar to the analogous case in Figure 7 the unstrained tether length is not chosen optimally, since the system does not really approach a relative equilibrium motion. Compared to the mission scenario presented in Figure 7 maximum values of controls in the r and θ directions decrease to 10 N and 9 N, respectively. Note the fairly large required control input peaks occurring at times when the system goes from a steady-spin motion to a tether deployment/retrieval motion or vice versa. This is only due to the non-smoothness of the chosen desired trajectory.

A more complex and thrust efficient tether length control law is obtained using equation (16), where the unstrained tether length is chosen to keep the TSS in a state corresponding to an instantaneous relative equilibrium at all times during the entire mission. Obtained simulation results are

illustrated in Figure 9. For this scenario we also included smoothing functions with a period of 40.0 s each. The specific tether length control law significantly decreases required control input in radial direction during the entire mission. The use of smoothing functions reduces peak control input in radial and angular direction during transition times. Also note that the error signals are reduced by about four orders of magnitude. Similar to the previously presented mission scenarios the control of the angular direction requires the bigger part of the overall control effort. In all the cases presented the magnitude of the angular momentum vector undergoes significant changes during tether deployment/ retrieval phases. For mission scenario 2, $\dot{\theta}_{i,d}$ and $\dot{r}_{i,d}$ are constant. Temporarily dropping index notation we see that with $h = \|\mathbf{h}\| \propto \dot{\theta}_{i,d} r^2$ the change in angular momentum is $(d/dt) h \propto r$ and the control force is linearly increasing during tether deployment and linearly decreasing during tether retrieval. In the case of mission scenario 3 the tangential velocity of the point masses $v = v_{max}$ is constant and $r \propto \sqrt{t + c_2}$. Therefore with $h \propto vr$ it is straightforward to show that $(d/dt) h \propto \dot{r} \propto 1/\sqrt{t + c_2}$.

We point out that for the current analysis the control power required to enforce the tether length/tension law has not been taken into account. This issue will have to be addressed in order to be able to make objective judgements on the performance of the particular overall control system.

SUMMARY AND CONCLUSIONS

Techniques to control the motion of a Tethered Satellite System (TSS) comprised of n point masses and interconnected by m idealized tethers are presented. Specifically, the control problem of a triangular and symmetrical TSS with $n = 3$ point masses and $m = 3$ tethers is considered. Several mission scenarios for NASA's SPECS mission are introduced and asymptotic tracking laws based on input-state feedback linearization are developed. Required thrust levels can be significantly decreased by using a tether length control law which keeps the system in a relative equilibrium during the entire mission.

The discontinuous character of the tethers introduces issues related to the application of the particular control technique used. Also, the proper implementation of coupled control including both point mass control and tether tension control will require further research to develop a comprehensive understanding of the overall power efficiency of the control system. Finally, we plan to refine the current system model to include rigid body dynamics of the spacecraft and a more complex tether model to simulate tether vibrations.

ACKNOWLEDGEMENTS

This work was supported by David Quinn of NASA Goddard Space Flight Center and by Arje Nachman of the Air Force Office of Scientific Research.

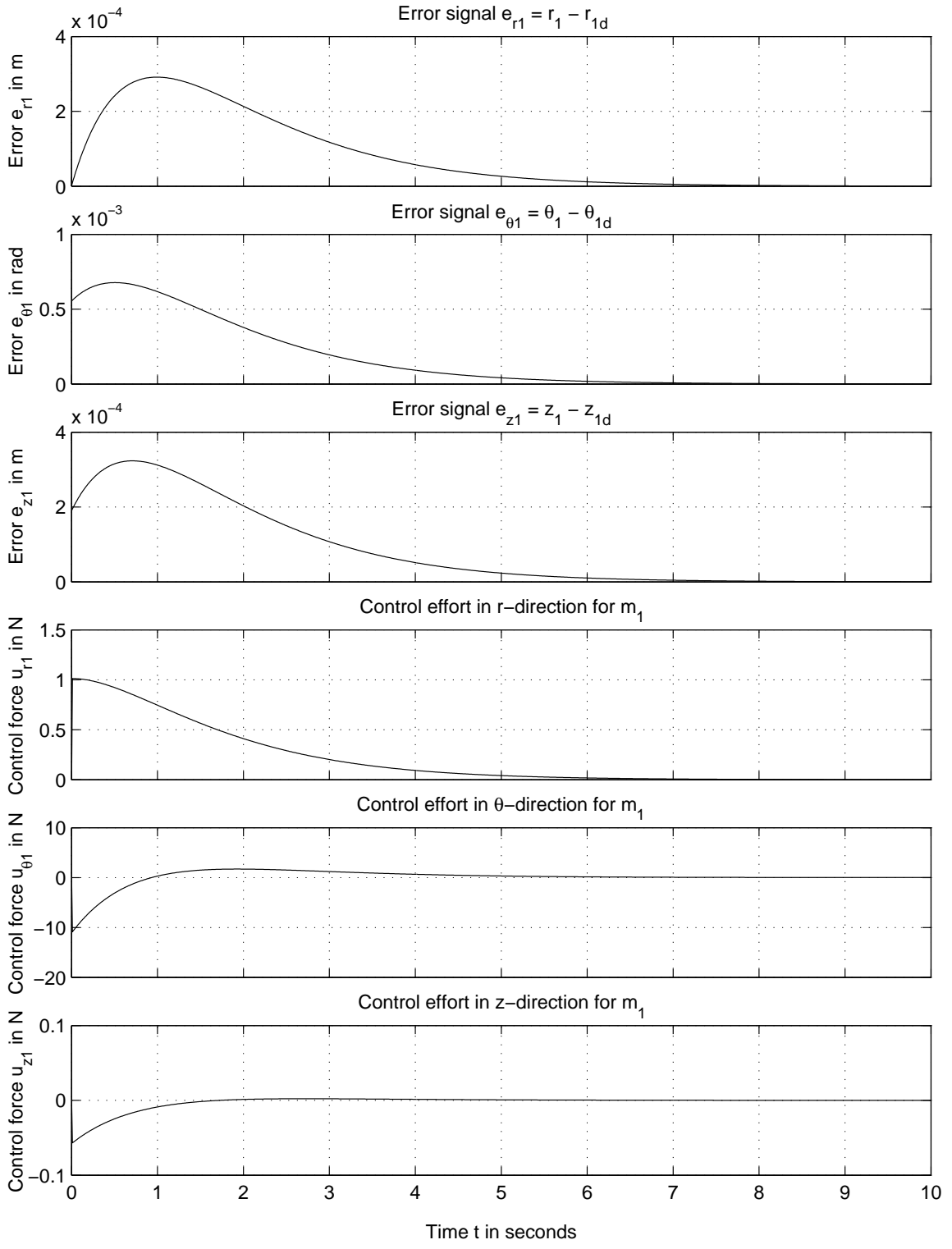


Figure 6: Output error and control vector time histories for an initial conditions perturbation response. The controlled system performs a relative equilibrium motion.

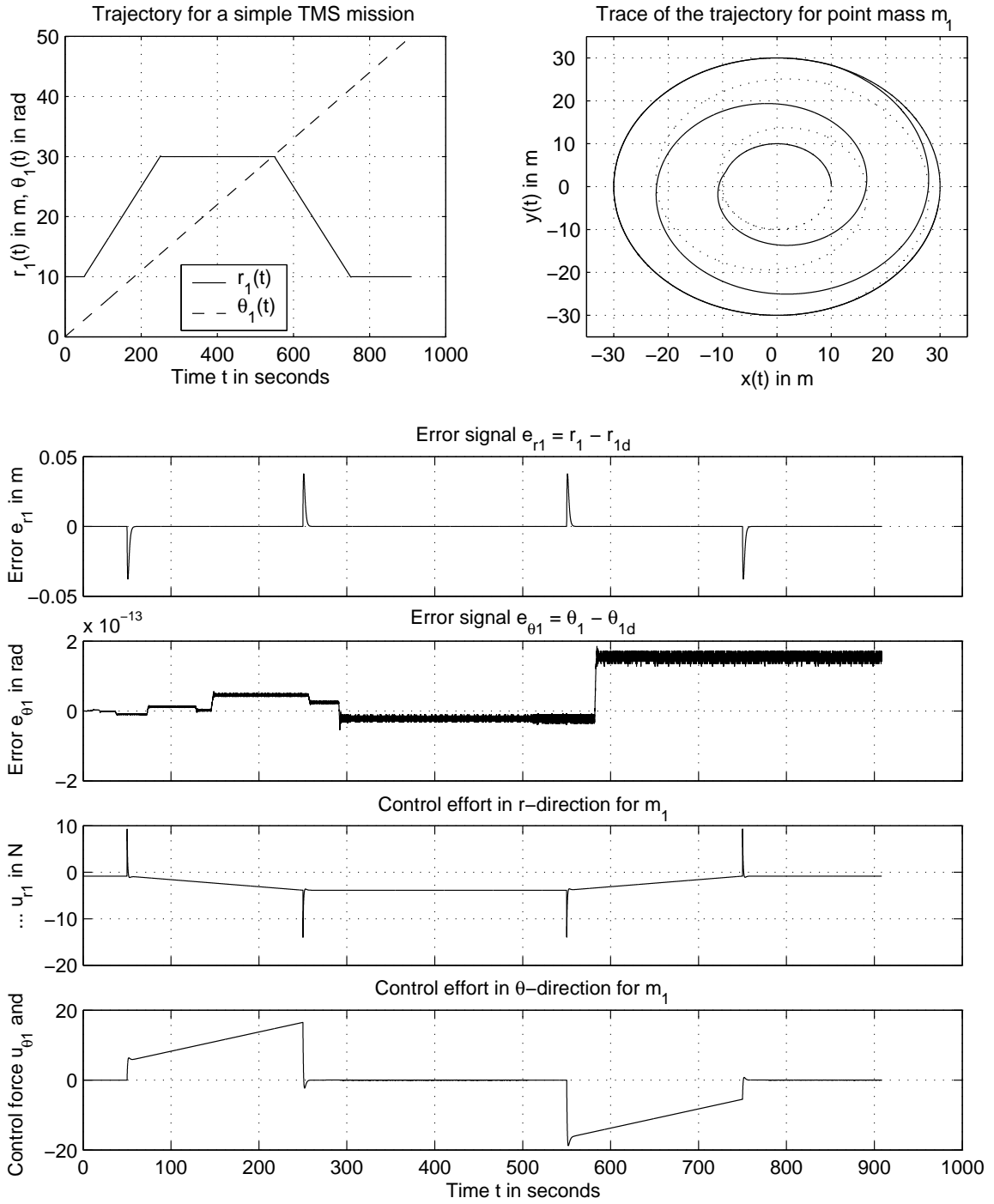


Figure 7: Trajectory of point mass m_1 (upper plots) and corresponding output error and control vector time histories for mission scenario 2 (lower plots).

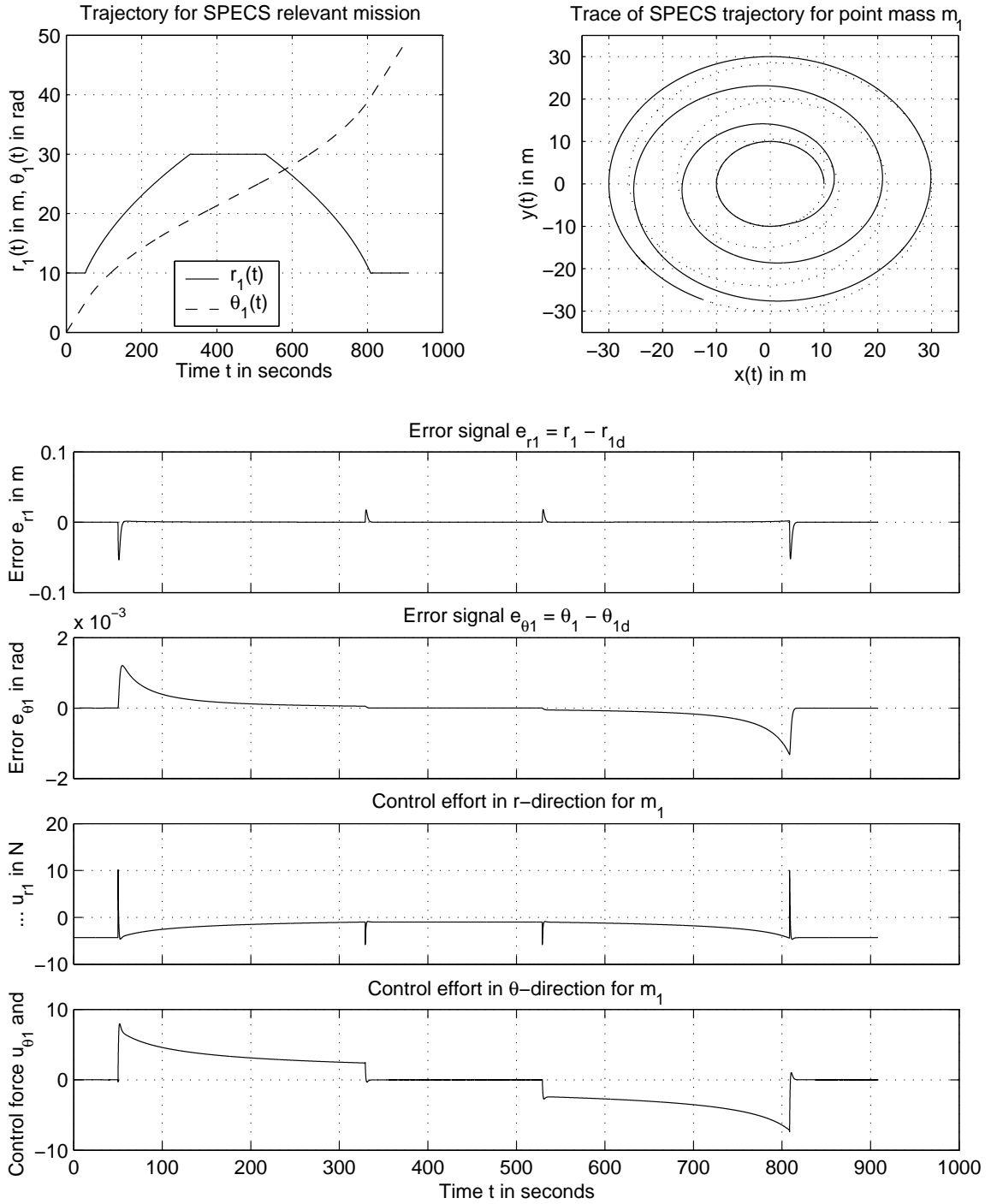


Figure 8: Trajectory of point mass m_1 (upper plots) and corresponding output error and control vector time histories for mission scenario 3 (lower plots).

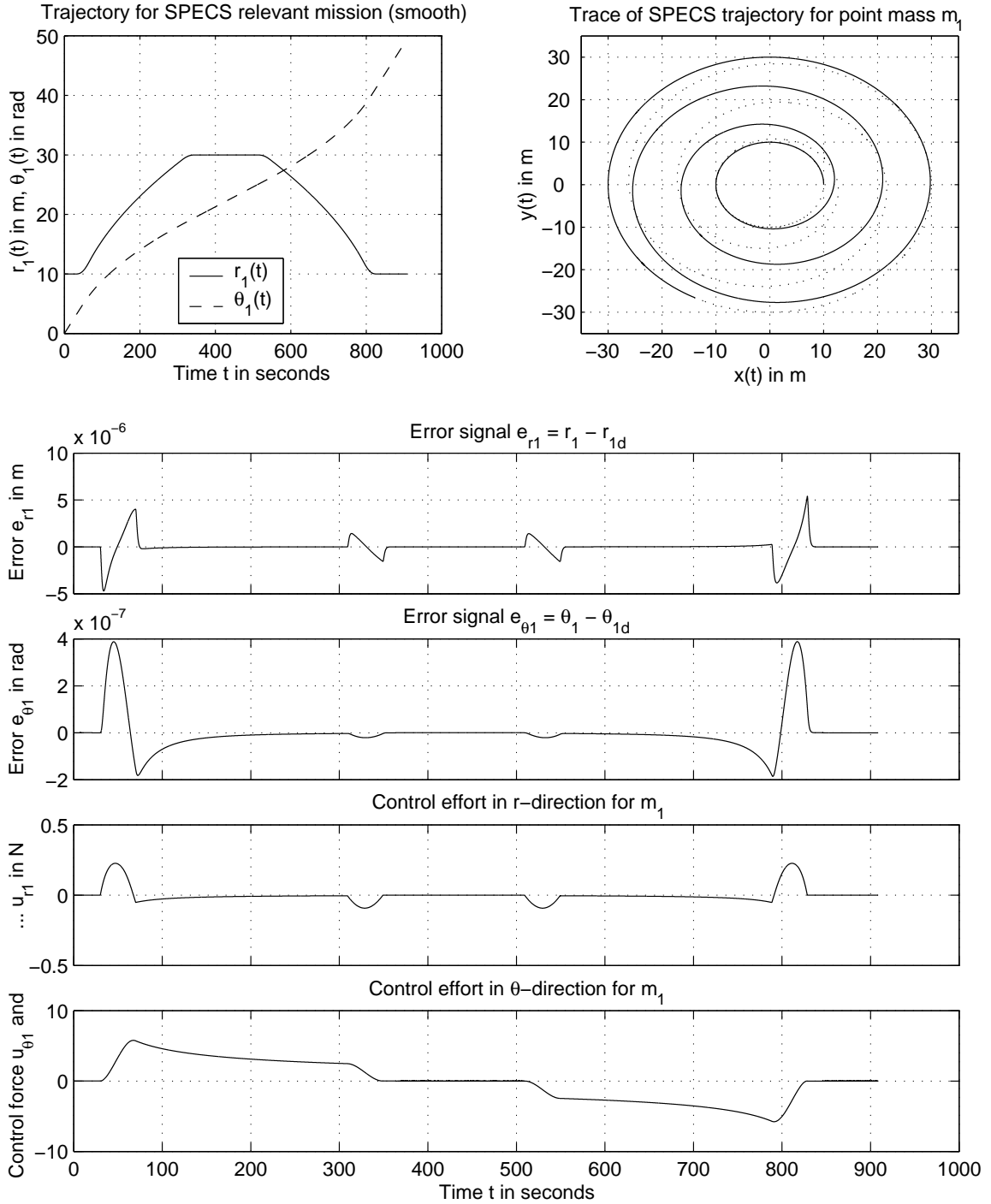


Figure 9: Smooth trajectory of point mass m_1 (upper plots) and corresponding output error and control vector time histories for mission scenario 3 (lower plots). The system is in a state corresponding to an instantaneous relative equilibrium at any point in time during the mission.

REFERENCES

- [1] JOHNSON, L., GLICHRIST, B., ESTES, R. D., and LORENZINI, E., “Overview of Future NASA Tether Applications,” *Advances in Space Research*, Vol. 24, No. 4, 1999, pp. 1055–1063.
- [2] MACCONE, C., “Tethered System to Get Magnified Radio Pictures of the Galactic Center From a Distance of 550 AU,” *Acta Astronautica*, Vol. 45, No. 2, 1999, pp. 109–114.
- [3] QUADRELLI, M. B., HADAEGH, F. Y., LORENZINI, E. C., and BOMBARDELLI, C., “Precision Tethered Formations for LEO and Space Interferometry Applications,” December 2001, 16th International Symposium on Space Flight Dynamics, Pasadena, California.
- [4] COSMO, M. and LORENZINI, E., *Tethers in Space Handbook*, Cambridge, Massachusetts, 3rd ed., 1997, prepared for NASA/MSFC by Smithsonian Astrophysical Observatory.
- [5] BELETSKY, V. V. and LEVIN, E. M., *Dynamics of Space Tether Systems*, Vol. 83 of *Advances in Astronautical Sciences*, Univelt, Incorporated, P.O. Box 28130, San Diego, California 92198, 1993.
- [6] QUINN, D. A. and FOLTA, D. C., “A Tethered Formation Flying Concept for the SPECS Mission,” *Proceedings of the 23rd Rocky Mountain Guidance and Control Conference, Breckenridge, Colorado*, Vol. 104 of *Advances in the Astronautical Sciences*, 2000, pp. 183–196.
- [7] KIM, M. and HALL, C. D., “Lyapunov and Halo Orbits About L_2 ,” *Proceedings of the 2001 AAS/AIAA Astrodynamics Specialist Conference, Quebec City, Canada*, Vol. 109 of *Advances in the Astronautical Sciences*, 2002, pp. 349–366.
- [8] BUROV, A. A. and TROGER, H., “The Relative Equilibria of an Orbital Pendulum Suspended on a Tether,” *Journal of Applied Mathematics and Mechanics*, Vol. 64, No. 5, 2000, pp. 723–728.
- [9] LIAW, D. C. and ABED, E. H., “Tethered Satellite System Stability,” Tech. Rep. SRC TR 89–21, Department of Electrical Engineering and the Systems Research Center, University of Maryland., 1989.
- [10] AKELLA, M. R., “Control Law Development for Tethered Formation Flying,” Tech. rep., Center for Space Research, The University of Texas at Austin, January 2001.
- [11] GATES, S. S., “Multi-tethered Space-based Interferometers: Particle System Model,” Tech. Rep. NRL/MR/8231–01-8579, Naval Research Laboratory, Washington, DC 20375-5320, September 2001.
- [12] DIGNATH, F. and SCHIEHLEN, W., “Control of the Vibrations of a Tethered Satellite System,” *Journal of Applied Mathematics and Mechanics*, Vol. 64, No. 5, 2000, pp. 715–722.
- [13] de MATTEIS, G. and de SOCIO, L. M., “A Discretized Model for the Dynamics of a Tethered Satellite System and Applications,” *Proceedings of the 1991 AAS/AIAA Space Flight Mechanics Meeting, Houston, Texas*, Vol. 75 of *Advances in the Astronautical Sciences*, 1991, pp. 1029–1052.
- [14] PRADHAN, S., MODI, V. J., and MISRA, A. K., “Tether-Platform Coupled Control,” *Acta Astronautica*, Vol. 44, No. 5, 1999, pp. 243–256.
- [15] KALANTZIS, S., MODI, V. J., and PRADHAN, S., “Dynamics and Control of Multibody Tethered Systems,” *Acta Astronautica*, Vol. 42, No. 9, 1998, pp. 503–517.

- [16] DECOU, A. B., "Attitude and Tether Vibration Control in Spinning Tethered Triangles for Orbiting Interferometry," *The Journal of the Astronautical Sciences*, Vol. 41, No. 3, July-September 1993, pp. 373–398.
- [17] DECOU, A. B., "Tether Static Shape for Rotating Multimass, Multitether, Spacecraft for Triangle Michelson Interferometer," *Journal of Guidance and Control*, Vol. 12, No. 2, March-April 1989, pp. 273–275.
- [18] MISRA, A. K., "Equilibrium Configurations of Tethered Three-Body Systems and their Stability," *Proceedings of the 2001 AAS/AIAA Space Flight Mechanics Meeting, Santa Barbara, California*, Vol. 108 of *Advances in the Astronautical Sciences*, 2001, pp. 1757–1772.
- [19] MISRA, A. K., AMIER, Z. E., and MODI, V. J., "Attitude Dynamics of Three-Body Tethered Systems," *Acta Astronautica*, Vol. 17, No. 10, 1988, pp. 1059–1068.
- [20] MISRA, A. K. and MODI, V. J., "Three-Dimensional Dynamics and Control of Tether-Connected N-Body Systems," *Acta Astronautica*, Vol. 26, No. 2, 1992, pp. 77–84.
- [21] KESHMIRI, M. and MISRA, A. K., "General Formulation for N -body Tethered Satellite System Dynamics," *Journal of Guidance, Control and Dynamics*, Vol. 19, No. 1, January-February 1996, pp. 75–83.
- [22] MISRA, A. K., BELLEROSE, J., and MODI, V. J., "Dynamics of a Tethered System near the Earth-Moon Lagrangian Points," *Proceedings of the 2001 AAS/AIAA Astrodynamics Specialist Conference, Quebec City, Canada*, Vol. 109 of *Advances in the Astronautical Sciences*, 2002, pp. 415–435.
- [23] FARQUHAR, R. W., "Tether Stabilization at a Collinear Libration Point," *The Journal of the Astronautical Sciences*, Vol. 49, No. 1, January-March 2001, pp. 91–106.
- [24] KHALIL, H. K., *Nonlinear Systems*, Prentice-Hall, Inc., Upper Saddle River, New Jersey, 3rd ed., 2002.
- [25] SASTRY, S., *Nonlinear Systems*, Springer-Verlag, New York, 1999.
- [26] SEPULCHURE, R., JANKOVIĆ, M., and KOKOTOVIĆ, P., *Constructive Nonlinear Control*, Springer-Verlag, London, 1st ed., 1997.
- [27] SLOTINE, J.-J. E. and LI, W., *Applied Nonlinear Control*, Prentice-Hall, Inc., Englewood Cliffs, New Jersey, 1991.
- [28] ISIDORI, A., *Nonlinear Control Systems*, Springer-Verlag, London, 3rd ed., 1995.
- [29] FRANKLIN, G. F. and POWELL, J. D., *Feedback Control of Dynamic Systems*, Electrical and Computer Engineering, Addison-Wesley Publishing Company, Inc., 3rd ed., 1994.